

Electrodynamical signatures of polaronic charge ordering.

S. Ciuchi

*Istituto Nazionale di Fisica della Materia and Dipartimento di Fisica
Università dell'Aquila, via Vetoio, I-67010 Coppito-L'Aquila, Italy*

S. Fratini

*Institut NEEL, CNRS & Université Joseph Fourier
BP 166, F-38042 Grenoble Cedex 9, France*

(Dated: March 22, 2019)

We apply dynamical mean field theory to study a prototypical model that describes charge ordering in the presence of both electron-lattice interactions and intersite electrostatic repulsion between electrons. We calculate the optical and d.c. conductivity, and derive approximate formulas valid in the limiting electron-lattice coupling regimes. In the weak coupling regime, we recover the usual behavior of charge density waves, characterized by a transfer of spectral weight due to the opening of a gap in the excitation spectrum. In the opposite limit of very strong electron-lattice coupling, instead, the charge ordering transition is signaled by a global enhancement of the optical absorption, with no appreciable spectral weight transfer. Such behavior is related to the progressive suppression of thermally activated charge defects taking place below the critical temperature. At intermediate values of the coupling within the polaronic regime, a complex behavior is obtained where both mechanisms of transfer and enhancement of spectral weight coexist.

I. INTRODUCTION

As opposed to conventional charge density waves,¹ that are well understood in terms of lattice-driven instabilities of the Fermi surface in metallic systems, there is no unified description of the charge ordering (CO) transitions observed in strongly interacting systems, or “bad metals”. Typical examples of such systems are transition-metal oxides, which are invariably characterized by a complex interplay between several microscopic interactions, involving the charge, spin, orbital and lattice degrees of freedom. This complexity seems to preclude the identification of a simple, common, charge ordering mechanism. Still, electron-lattice interactions are always present to some extent, and often play a dominant role in driving the CO transition in these systems. Charge ordering phenomena involving a strong electron-lattice coupling have been found in manganites,^{2,3,4} nickelates,^{5,6} layered cobaltates,^{7,8} magnetite,^{9,10,11} vanadates,^{12,13} oxoborates,¹⁴ as well as in other low-dimensional systems.^{15,16}

In this work we focus on a minimal model which describes charge ordering in the presence of electron-lattice interactions, with particular attention to the polaronic regime obtained at strong coupling. The model consists of electrons on a bipartite lattice, at a commensurate concentration of one electron on every two sites, interacting locally with dispersionless lattice vibrations. The electrons also interact mutually via an intersite electrostatic repulsion, which can be thought of as the screened part of the long-ranged Coulomb potential. While this oversimplified model only retains part of the complex physics involved in real systems, its solution can be helpful to clarify certain aspects of the charge ordering phenomena that are common to systems with strong electron-lattice interactions, and that can in principle be identified ex-

perimentally. To be specific, we solve the model by performing the following approximations:

(i) The magnetic degrees of freedom are taken out of the game by resorting to spinless electrons. This enforces locally the constraint of no double occupancy characteristic of the limit of strong “Hubbard” (on-site) repulsion. It is appropriate for our purposes, as long as we do not aim at describing the effects of electronic correlations on the low-energy physics, such as the existence of a quasi-particle peak or the induced magnetic exchange. In principle, this approximation is viable as long as the magnetic and charge degrees of freedom are governed by different energy scales. In such case, the magnetic interactions are not expected to have a strong influence on the charge ordering pattern (although exceptions do exist^{17,18,19}). This separation of energy scales is realized for instance in magnetite (Fe_3O_4),²⁰ where the CO transition occurs within a ferromagnetic phase that preexists at a much higher temperature. More examples can be found in systems (such as V_3O_5)¹³ where the CO transition takes place within a paramagnetic phase, the magnetic order setting in at a much lower temperature. The spinless approximation is also relevant to half-metals such as the colossal magnetoresistance manganites.

(ii) We consider a single electronic band, which rules out the orbital degrees of freedom and their possible ordering, that is known to play an important role in specific compounds.

(iii) The lattice vibrations are assumed adiabatic, i.e. their characteristic energy is much smaller than the electronic bandwidth, which is typically the case in transition-metal oxides. The adiabatic approximation is enforced here by treating the lattice degrees of freedom as static variables with a given (thermal) statistical distribution. As a consequence, the low-energy spectral features that derive from the quantum nature of the phonons

are lost. These would appear at energies comparable to, or below the phonon energies. Such features are anyhow of minor quantitative importance in the polaronic regime of interest here, where most of the spectral weight is moved to higher energies, of the order of the polaron binding energy. The same argument justifies the neglect of low-energy phenomena originating from electronic correlations as discussed at point (i) above, in all cases where the polarons set the dominant energy scale.

(iv) We apply single-site Dynamical Mean Field Theory (DMFT), appropriately adapted^{17,21,22,23} to account for the charge unbalance between neighboring sites in the charge ordered state. This approach is known to deal very effectively with local interaction mechanisms, regardless of their strength. It is therefore expected to give an accurate description of the electron-lattice physics. As was shown in Ref. 23, this approach correctly describes the crossover between the weak coupling charge density wave regime and strong-coupling polaronic regime, and allows to shed light on the role played by defects of the lattice polarization at the ordering transition. A lesser accuracy is achieved in treating the inter-site Coulomb repulsion, since non-local interactions reduce to the mean-field (Hartree) level in single-site DMFT. This is however not a primary limitation^{17,18} in the regime we are mainly interested in, where the physics is dominated by the electron-lattice interaction.

The main result of this work is the identification of qualitatively different behaviors of the electrodynamic response in the two fundamentally distinct regimes of charge ordering, governed by the strength of the electron-lattice interaction. In the weak coupling regime, the electrodynamic response is dominated by the opening of an energy gap in the excitation spectrum of an otherwise metallic system. At the ordering transition, the optical spectral weight is transferred from the Drude peak to the region above the gap, and the d.c. conductivity acquires a semiconducting character. On the contrary, in the strong coupling limit, a local charge segregation is already present in the normal phase, due to the formation of self-localized polarons. Correspondingly, the low energy spectrum is already strongly depleted by a polaronic “pseudo-gap”, and the genuine gap opening occurring at the transition does not give rise to any appreciable depletion or shift of the low frequency spectral weight. Instead, the ordering of polarons results in a global enhancement of the optical spectral weight, which is opposite to what is expected from a conventional charge density wave. The two scenarios described above coexist in the polaronic regime at moderate values of the electron-lattice coupling. This leads to a complex behavior presenting both a transfer and an enhancement of the spectral weight, resulting in a non-monotonic temperature dependence of the total optical weight within the CO phase. The inclusion of a direct intersite Coulomb interaction extends this complex intermediate region to larger electron-lattice interaction strengths.

The solution for the one-particle spectral function has

already been published in Ref. 23, in a model with electron-lattice interactions alone. Here we extend that treatment to calculate the optical and d.c. conductivity throughout the parameter space, including an intersite Coulomb repulsion between electrons. We also derive analytical expressions for these quantities that are valid in the polaronic regime, elucidating the role played by charge defects in both optical absorption and charge transport. It can be noted that an analogous model, without the Coulomb interaction term, was studied variationally in Ref. 24. There, however, the physics of defects was not addressed.

The paper is organized as follows. The general formalism for treating the charge ordered, broken-symmetry phase within the DMFT is presented in Sec. II. The equations are solved numerically in Sec. III. The optical and d.c. conductivity are calculated in Sec. IV and V respectively, making use of the Kubo formula. The results are discussed in Sec. VI.

II. MODEL AND SELF-CONSISTENT SOLUTION

We consider the following Hamiltonian:

$$H = -\frac{t}{\sqrt{z}} \sum_{\langle ij \rangle} (c_i^\dagger c_j + h.c.) + \frac{1}{2} k X_i^2 \quad (1)$$

$$+ g \sum_i (c_i^\dagger c_i - n) X_i + \frac{V}{2z} \sum_{\langle ij \rangle} (n_i - n)(n_j - n)$$

where the operator $c_i^\dagger(c_i)$ creates (destroys) a spinless electron at site i , n is the average electron density per site and X_i are the displacements of local oscillator modes, that are coupled to the local electron density via the parameter g . The electrons interact mutually via a nearest neighbor repulsion term V . The scaling of the repulsive term is chosen in such a way that the energy cost for a deviation from perfect charge ordering (i.e. flipping an occupied and an empty site) equals V . The scaling of the kinetic term t/\sqrt{z} yields a finite free-electron bandwidth in the limit of infinite connectivity (number of nearest neighbors $z \rightarrow \infty$). We shall consider for simplicity a semi-elliptical density of states (DOS) of half-width $D = 2t$, corresponding to a Bethe lattice of infinite connectivity. Nevertheless, the present calculation scheme can be easily generalized to other model DOS, to include more realistic band structures as obtained for example from ab-initio calculations of specific systems. We shall specialize to the commensurate concentration $n = 1/2$, which is equivalent to a quarter-filled band in the case of electrons with spin. In the present spinless case, the chemical potential is fixed at $\mu = 0$ from particle-hole symmetry.

An order parameter for the CO transition can be defined as the charge dimerization

$$\Delta n = n_A - n_B, \quad (2)$$

which varies between 0 and 1, the average density being given by $n = (n_A + n_B)/2 = 1/2$ (here A and B label respectively the charge-rich and charge-poor sublattices). The formalism needed to treat the electron-phonon interaction was set up in Ref. 23 by mapping the original lattice problem onto a pair of coupled impurity models. In the limit of infinite connectivity, any additional non-local interaction term self-averages to its mean-field (Hartree) value. Therefore, the extra Coulomb term can be straightforwardly included via a site dependent chemical potential shift in the Weiss fields, i. e. the local fields that take into account the effects of the electron itinerancy. On the Bethe lattice, the new Weiss fields read:

$$(G_0^{-1})^A = i\omega_n + \frac{V}{2}\Delta n - \frac{D^2}{4}G^{BB} \quad (3)$$

$$(G_0^{-1})^B = i\omega_n - \frac{V}{2}\Delta n - \frac{D^2}{4}G^{AA}. \quad (4)$$

It can be observed by direct inspection of Eqs. (3-4) that the Coulomb interaction does not affect the properties of the system in the normal phase (where $\Delta n = 0$), which is a drawback of the present approximation.

The above system of equations is closed self-consistently by expressing the site-diagonal propagators G^{AA} and G^{BB} in terms of the self-energy arising from the local interaction with the static phonon field:

$$G^{AA} = \int dX \frac{P_A(X)}{(G_0^{-1})^A - gX}, \quad (5)$$

and similarly for G^{BB} . Here $P_A(X)$ and $P_B(X)$ are the probability distribution functions (PDF) for the phonon displacements on the A and B sublattices, which can be expressed as functionals of the local electronic propagators in Matsubara frequencies (ω_n)²³

$$P_A(X) \propto e^{-\beta kX^2/2} \pi_n \{ [(G_0^{-1})^A - gX] / i\omega_n \}. \quad (6)$$

The numerical solution is achieved by successive iterations of the above equations, starting from a given ansatz for the sublattice propagators G^{AA} and G^{BB} . In the following we shall take the half-bandwidth D as the unit of energy.

We now briefly analyze the phase diagram obtained from the DMFT solution of the model Eq. (1). Fig. 1 shows the critical temperature for the charge ordering transition as a function of the electron-phonon coupling parameter $\lambda = g^2/2kD$, defined as the polaron energy $E_P = g^2/2k$ in units of the half-bandwidth. At $V = 0$, we recover the bell-shaped result obtained in Ref. 23. Such bell shape originates from the different mechanisms that drive the charge ordering in the two limiting regimes of small and large λ . At weak coupling, the critical temperature monotonically *increases* with the electron-phonon coupling, i.e. the same qualitative trend predicted by the usual BCS theory.⁴⁴ In this regime, the charge segregation and the long-range order take place

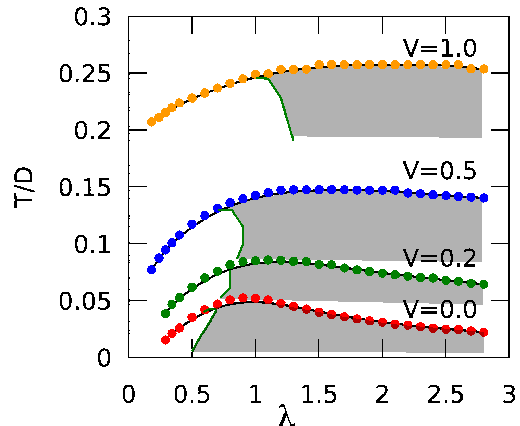


FIG. 1: Critical temperature delimiting the CO phase as a function of $\lambda = g^2/2kD$, for different values of V/D . Shaded areas below T_c mark polaronic regions where defects are present. The existence of defects is tracked by looking at metastable minima of the adiabatic potentials $V_{A,B} = -T \log(P_{A,B})$.

simultaneously at T_c . At strong coupling instead, due to polaron formation, *local* charge segregation occurs at a temperature $T \approx E_P$, much larger than ordering temperature T_c itself. The actual critical temperature T_c marks the onset of spatial ordering of such randomly distributed polarons. It is proportional to the “charge superexchange” $J = D/(4\lambda)$ and therefore *decreases* as the electron-phonon coupling increases. The asymptotic strong coupling expression for the critical temperature is $T_c = D/(16\lambda)$. From the above discussion we see that the maximum of T_c , obtained at $\lambda \approx 1$ for $V = 0$, signals the crossover between the weak-coupling and the polaronic behavior.

The ordered phase below T_c is also qualitatively different depending on the value of the electron-phonon coupling. In particular, in the strong coupling regime, the preexisting polarons progressively order upon lowering the temperature, and only attain a perfect alternate order at $T = 0$. At any finite temperature, a certain number of defects exist within the CO phase, in the form of charges localized on the “wrong” sublattice. The existence of such thermally-induced defects is intimately related to the existence of local lattice distortions in the normal phase, i.e. polaron formation.²³ We can therefore identify the existence of a *polaronic* CO phase, as opposed to the weak-coupling charge density wave, as the phase in which these defects are present.

The defect phase can be quantitatively characterized by analyzing the sublattice PDF’s, which acquire a bimodal structure for sufficiently large λ . More efficiently, one can look for the existence of two non-degenerate minima in the sublattice adiabatic potentials defined as $V_{A,B} = -T \log P_{A,B}$. The result of this procedure is illustrated by the shaded areas in the phase diagram of Fig. 1. We see that the defect phase emerges right at the

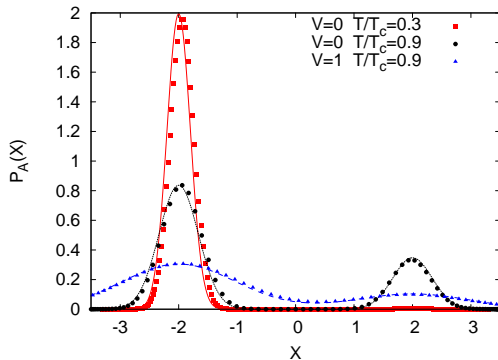


FIG. 2: Sublattice phonon PDF at $\lambda = 2$. The different curves are for $V = 0$ ($T/T_c = 0.3$ and 0.9) and $V = 1$ ($T/T_c = 0.9$). Points correspond to the DMFT self-consistent solution, lines represent the strong coupling theory Eq. (B5). The locus and shape of the peaks does not depend explicitly on V .

polaron crossover, i.e. in the region below the maximum of T_c vs λ .

Including a direct intersite repulsion clearly favors both types of charge ordering, as it increases T_c for all values of λ (compare the different curves in Fig. 1). Still, the evolution of the phase diagram with V suggests a non-trivial interplay between the direct Coulomb repulsion and the polaronic physics, as a finite V shifts the polaron crossover (as well as the boundary of the defect phase) towards larger values of λ . It can be argued that, by treating the intersite Coulomb interaction beyond mean-field, charge fluctuations of the same nature of the lattice defects evidenced above could start playing a role.²⁵ For this reason, in the following we shall restrict to the regime of small to moderate V , where the dominant physics is set by the electron-phonon interactions, therefore suppressing the fluctuations of the Coulomb interaction term.

The sublattice PDF $P_A(X)$ evaluated at $\lambda = 2$, well inside the polaronic regime, is shown in Fig. 2. Defects in the A sublattice give rise to a minority peak of opposite “polarization” with respect to the preferred one. The area of the minority peak can be used to define the number of defects (n_d) in the CO phase. In the strong coupling regime, it tends to $1/2$ at $T = T_c$, where the two peaks become equivalent (polarons are randomly distributed over the two sublattices), while it vanishes exponentially at $T = 0$, when perfect charge ordering is achieved. This occurs because, as the temperature is reduced, the population of the metastable minimum of the potentials $V_{A,B}$ is progressively depleted, leading to an exponential reduction of n_d . It should be noted that the possibility of strictly $n_d = 0$ is related to our classical treatment of the lattice degrees of freedom, which breaks down at temperatures much smaller than the characteristic phonon energies. Properly including phonon quantum fluctuations⁴³ would lead to the appearance of charge defects even in the zero temperature limit.

In the limit $\lambda \rightarrow \infty$, the number of defects is related

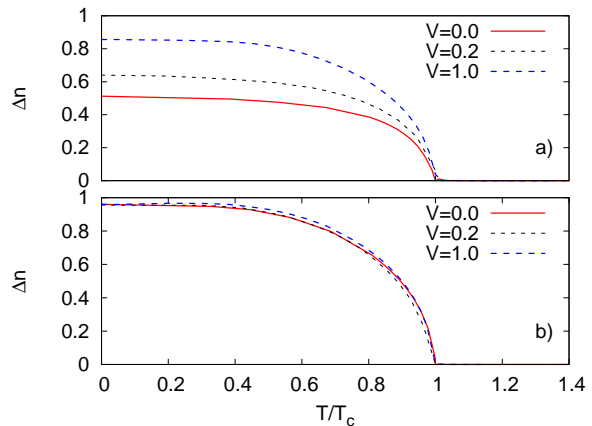


FIG. 3: Evolution of the charge dimerization for $\lambda = 0.4$ (a) and for $\lambda = 2.0$ (b), at different values of V .

to the order parameter through

$$\Delta n = 1 - 2n_d. \quad (7)$$

At finite λ in the polaronic phase ($\lambda \gtrsim 1$), the above Eq. (7) has to be replaced by $\Delta n = (1 - 2n_d)[1 - 1/(8\lambda^2) + \dots]$, which properly accounts for the fact that the charge dimerization Δn does not strictly tend to 1 even when the polarons are perfectly ordered ($n_d = 0$). This is because at finite λ the electronic wavefunction is not fully localized and acquires a finite extension on the neighboring sites, which necessarily pertain to the minority sublattice.

The evolution of the charge dimerization with T in different regions of the phase diagram is reported in Fig. 3. In the polaronic regime, Δn is a universal function of T/T_c , independent of V , as shown in Fig. 3.b. This means in particular that the number of defects n_d is a function of T/T_c alone, and V only enters implicitly through the determination of T_c . Interestingly, the gap ratio $\Delta_{T=0}/T_c$ can become very large in the polaronic regime, due to the preexisting pseudogap $\Delta \propto E_P \gg T_c$.²³ In the opposite weak electron-phonon coupling limit, we recover a BCS-like behavior for Δn . In that case the gap is given by $\Delta = (\lambda D + V/2)\Delta n$. Its value at $T = 0$ satisfies the mean-field ratio $\Delta_{T=0}/T_c = 3.54$. It is worth noting that this limit is only reached asymptotically as $\lambda \rightarrow 0$. For small but finite λ , T_c is dramatically reduced by thermally induced lattice fluctuations,^{23,26} while $\Delta_{T=0}$ is not. Therefore the gap/ T_c ratio rapidly increases with λ even well outside the polaronic region.

III. OPTICAL CONDUCTIVITY

A. DMFT formulation

We now derive the Kubo formula for the optical conductivity in the CO phase. To this aim we develop a general formalism which makes explicit use of translational

invariance as in the hypercubic lattice, following the lines of Ref. 27. In this framework it is possible to write expressions for the electron propagators in k -space. This is achieved through a canonical transformation that defines new electron creation operators $c_{\mathbf{k}}^{A,B} = (c_{\mathbf{k}} \pm c_{\mathbf{k}+\mathbf{Q}})/\sqrt{2}$, where $\mathbf{Q} = (\pi, \pi, \dots)$ is the instability wave vector in any dimensions and \mathbf{k} spans the reduced Brillouin zone (RBZ). With the above transformation, the tight binding term becomes $\sum_k^{RBZ} \epsilon_{\mathbf{k}} (c_{\mathbf{k}}^{\dagger A} c_{\mathbf{k}}^B + c_{\mathbf{k}}^{\dagger B} c_{\mathbf{k}}^A)$, where $\epsilon_{\mathbf{k}}$ is the original non-interacting band dispersion. The fully interacting fermion propagators on the bipartite lattice can be defined as the matrix elements

$$G_{\mathbf{k}}^{\alpha\beta} = -i \langle T c_{\mathbf{k}}^{\alpha}(t) c_{\mathbf{k}}^{\beta}(0) \rangle \quad (\alpha, \beta = A, B) \quad (8)$$

of the 2×2 matrix $\hat{G}_{\mathbf{k}}$. The corresponding spectral functions are given by $\hat{\rho}(\mathbf{k}, \omega) = -Im \hat{G}_{\mathbf{k}}(\omega)/\pi$. Once the local self-energies on the two sublattices are known from the solution outlined in Sec. II, the Green's functions of Eq. (8) are obtained by inverting the matrix

$$\hat{G}_{\mathbf{k}}^{-1} = \begin{pmatrix} z^A & -\epsilon_{\mathbf{k}} \\ -\epsilon_{\mathbf{k}} & z^B \end{pmatrix} \quad (9)$$

with $z^A = \omega + i\delta + \mu - \Sigma_A(\omega)$, and similarly for z^B .

In the tight binding model of Eq. (1), the current operator along a given (say x) direction reads

$$J_x = -i \frac{t}{\sqrt{z}} \sum_{i, \hat{\delta}} \delta_x c_{i+\hat{\delta}}^{\dagger} c_i, \quad (10)$$

where the sum extends over all sites i of the lattice and their z nearest neighbors, identified by the vectors $\hat{\delta}$. Transforming to the sublattice operators, the current operator can be expressed as:

$$J_x = -i \sum_{\mathbf{k} \in RBZ} v_{\mathbf{k}} (c_{\mathbf{k}}^{\dagger A} c_{\mathbf{k}}^B + c_{\mathbf{k}}^{\dagger B} c_{\mathbf{k}}^A). \quad (11)$$

In a hypercubic lattice, only the two neighbors along the x direction contribute to the above sum, and the corresponding current vertex is $v_{\mathbf{k}} = 2 \frac{t}{\sqrt{z}} \sin k_x$.

In the context of DMFT, due to the vanishing of vertex corrections^{28,29,30} the current-current correlation function can be expressed exactly in terms of single particle

Green's functions. This simplification still holds in the broken-symmetry phase because the $\mathbf{k} \rightarrow -\mathbf{k}$ symmetry is preserved even in the reduced Brillouin zone. Reminding the definitions Eq.(8), we can write the current-current correlation function as

$$\langle T J_x(t) J_x(0) \rangle = \sum_{\mathbf{k} \in RBZ} v_{\mathbf{k}}^2 Tr \left[\tau_x \hat{G}_{\mathbf{k}}(t) \tau_x \hat{G}_{\mathbf{k}}(-t) \right] \quad (12)$$

where we have made use of the Pauli matrix τ_x to obtain a compact expression. The trace is performed in the sublattice indices A, B .

The optical conductivity follows from the Kubo formula, upon transforming the current-current correlation function to the frequency domain:

$$\sigma(\omega) = \sigma_0 \int_{RBZ} d\epsilon N(\epsilon) \phi(\epsilon) \times \int_{-\infty}^{\infty} d\nu Tr [\tau_x \hat{\rho}(\epsilon, \omega + \nu) \tau_x \hat{\rho}(\epsilon, \nu)] \frac{f(\nu) - f(\nu + \omega)}{\omega}. \quad (13)$$

In the above equation, the constant $\sigma_0 = \pi e^2 a^2 / \hbar v$ carries the dimensions of conductivity, a being the lattice spacing, v the volume of the unit cell, $f(\nu) = [1 + e^{\beta(\nu - \mu)}]^{-1}$ the Fermi function and $\hat{\rho}$ the spectral functions associated to sublattice propagators \hat{G} . Taking advantage of the local nature (k -independence) of the self-energy, the sum over momenta in Eq. (12) has been replaced by an integration over energies, weighted by the DOS $N(\epsilon)$ and the current vertex $\phi(\epsilon)$ of the non-interacting lattice. Use has also been made of the fact that $v_{\mathbf{k}}^2$ is invariant under the transformation $\mathbf{k} \rightarrow \mathbf{k} + \mathbf{Q}$. The integration over the band dispersion ϵ in the current-current correlation function can be performed analytically, leading to:

$$\sigma(\omega) = \sigma_0 \int_{-\infty}^{\infty} d\nu B(\nu + \omega, \nu) \frac{f(\nu + \omega) - f(\nu)}{\omega}. \quad (14)$$

The function B is defined as:

$$B(\nu + \omega, \nu) = -\frac{1}{4\pi} Re \left\{ \chi(z_1^A, z_1^B; z_2^A, z_2^B) - \chi(z_1^A, z_1^B; z_2^{A*}, z_2^{B*}) \right\} \quad (15)$$

where

$$\chi(z_1^A, z_1^B; z_2^A, z_2^B) = \frac{2}{\xi_1^2 - \xi_2^2} \left\{ \frac{\mathcal{K}(\xi_2)}{\xi_2} [z_1^B z_2^A + z_1^A z_2^B + 2\xi_2^2] - \frac{\mathcal{K}(\xi_1)}{\xi_1} [z_1^B z_2^A + z_1^A z_2^B + 2\xi_1^2] \right\} \quad (16)$$

and

$$z_1^{\alpha} = \omega + \nu + i\delta - \Sigma_{\alpha}(\omega + \nu) \quad (17)$$

$$z_2^{\alpha} = \nu + i\delta - \Sigma_{\alpha}(\nu) \quad (18)$$

$$\xi_1 = \sqrt{z_1^A z_1^B} \quad (19)$$

$$\xi_2 = \sqrt{z_1^A z_2^B} \quad (20)$$

with $\alpha = A, B$ the sublattice index. The function \mathcal{K} is

the Hilbert transform of the product $N(\epsilon)\phi(\epsilon)$, that can be evaluated analytically in the case of a semi-elliptical DOS. For this we take the following form of the current vertex $\phi(\epsilon) = (D^2 - \epsilon^2)/3$. This is chosen in such a way as to fulfill the f-sum rule^{31,32,36} which relates the total optical spectral weight

$$W = \int_0^\infty d\omega \sigma(\omega). \quad (21)$$

to the kinetic energy of the interacting system. The demonstration of the f-sum rule in the broken-symmetry phase is explicitly carried out in Appendix C.

In the following Sections we shall analyze separately the results in the weak electron-phonon coupling regime $\lambda \lesssim 1$, in the extreme strong coupling limit $\lambda \gg 1$, and in the most interesting polaronic regime $\lambda \gtrsim 1$.

B. Weak coupling regime, $\lambda \lesssim 1$

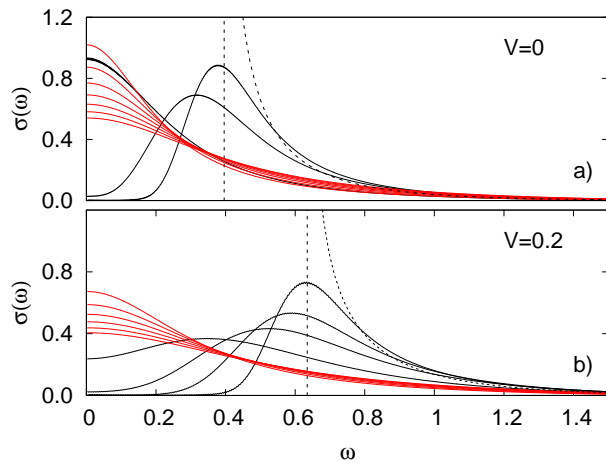


FIG. 4: (color online) Optical conductivity at $\lambda = 0.4$, $V = 0$ (a) and $V = 0.2D$ (b). The curves in panel (a) are at equally spaced temperatures in the range $T/T_c = 0.4 - 2.9$ ($T_c = 0.026D$) and in panel (b) $T/T_c = 0.2 - 1.5$ ($T_c = 0.052D$). Curves corresponding to the disordered phase at $T > T_c$ are in red. The dashed line is the mean-field result Eq. (A2) at the lowest temperature.

In figure 4 we report the results for the optical conductivity at $\lambda = 0.4$, for different values of the intersite Coulomb interaction V . At such a moderate value of the electron-lattice coupling, although the overall behavior qualitatively agrees with what is expected in the conventional mean-field scenario (see Appendix A, and the dashed lines in Fig. 4), the spectral features are appreciably smoothed by the presence of lattice fluctuations. A measure of such broadening is provided by the variance $s = \sqrt{2E_P T}$ of the energy fluctuations of the phonon field,³⁴ which is of the order of $0.1D$ in the example of Fig. 4. This is a sizable fraction of the electronic bandwidth, which is however sufficiently small that the overall

band picture remains qualitatively valid at temperatures comparable or below T_c , which are the ones of interest here.

Due to the classical approximation for the phonons, the Drude peak in the normal phase is replaced by an incoherent gaussian peak around $\omega = 0$,³⁵ whose width is proportional to s . Below the critical temperature, a finite charge dimerization develops (cf. Fig. 3) which is reflected in the optical spectra through a progressive gap opening. Correspondingly, the low-frequency spectral weight is transferred to frequencies above the optical gap located at $\Delta_{opt} \simeq (2\lambda D + V)\Delta n$. The sharp square-root divergence at $\omega = \Delta_{opt}$ expected from the standard mean-field treatment (dashed line, corresponding to Eq. A2) is also smoothed due to the presence of thermal lattice fluctuations. These are also responsible for the subgap absorption tail observed in Fig. 4, which is absent in the mean-field result. A similar scenario can also arise at $T = 0$ from quantum lattice fluctuations, as shown in Ref. 24.

The effect of a finite V is to strengthen the CO phase, without modifying the broadening of the spectral features. The optical gap increases both due to the increased value of the charge dimerization Δn (see Fig.3), and to the explicit contribution $V\Delta n$, which represents the extra electrostatic cost to move one particle from one sublattice to the other.

C. Strong coupling limit, $\lambda \gg 1$

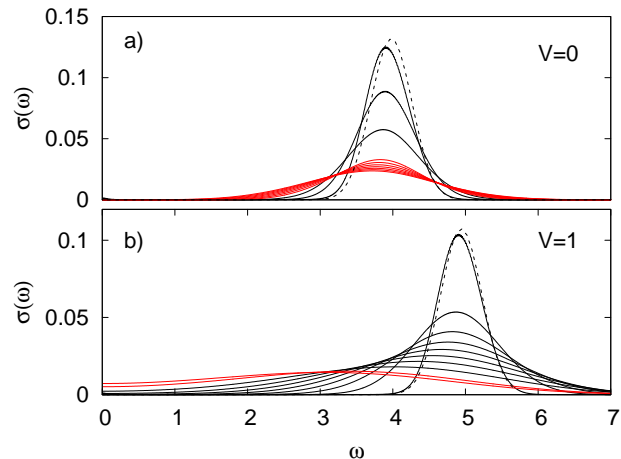


FIG. 5: (color online) Optical conductivity at $\lambda = 2$, $V = 0$ (a) and $V = 1$ (b). The curves in panel (a) are at equally spaced temperatures in the range $T/T_c = 0.3 - 2.5$ ($T_c = 0.031D$) and in panel (b) $T/T_c = 0.04 - 1.1$ ($T_c = 0.26D$). Curves corresponding to the disordered phase at $T > T_c$ are in red. The dashed line is the strong coupling result Eq. (B7) at the lowest temperature.

The results for the optical absorption in the strong coupling limit are shown in Fig. 5 for $\lambda = 2$. The behavior

is very different from the weak coupling regime analyzed previously. This is seen already in the normal phase, where the Drude peak is replaced by a broad peak at finite frequency. This peak arises due to the formation of small polarons, and reflects the optical transitions within the polaron internal structure. The peak position scales with the polaron energy roughly as $\omega \approx 2E_P$, and its width is again proportional to the spread s of the lattice fluctuations.

Because the low-frequency spectral weight is already strongly suppressed in the normal phase, no clear gap opening is visible at T_c . Indeed, in Fig. 5.a. ($\lambda = 2$, $V = 0$) there is no visible depletion of the optical conductivity at low frequency (apart from the natural evolution of the peak width governed by s) and no clear shift of the position of the polaron peak as the temperature is reduced below T_c . Rather, the ordering transition leads to a sharp increase of the spectral weight associated to the polaronic peak. As we demonstrate hereafter, this increase is a direct consequence of the suppression of charge defects, and constitutes a distinctive signature of the polaronic charge ordering.

The observed behavior can be understood by noting that in the normal phase, only half of the sites neighboring a given polaron are unoccupied, and therefore available for an optical transition as induced by the current operator Eq. (10). The number of available empty neighbors increases as charge defects are progressively removed below T_c , and so does the weight of the polaronic absorption peak, until each polaron becomes exclusively surrounded by unoccupied sites at $T = 0$. The above analysis can be carried out in general to show that the probability for polaronic optical transitions is proportional to $n_A(1 - n_B)$ (for polarons in sublattice A) and $n_B(1 - n_A)$ (for polarons in sublattice B). The sum scales as $(1 + \Delta n^2)$, leading to an increase of up to a factor of 2 of the optical spectral weight in the CO phase.

A more detailed discussion of the spectral weight enhancement is provided in Appendix B, where we derive analytical expressions for the optical conductivity valid at large λ . We report here the formula appropriate in the CO phase at $V = 0$, which is simply expressed in terms of the normal state polaron absorption $\sigma_{norm}(\omega)$ as

$$\sigma(\omega) = 2[1 - 2n_d(1 - n_d)]\sigma_{norm}(\omega). \quad (22)$$

This equation directly relates the observed enhancement of the polaron peak with the suppression of the number of defects, in agreement with the qualitative argument given above, as can be easily shown using Eq. (7) above. Both this expression and its analog Eq. (B8) valid at $V \neq 0$ describe very accurately the full DMFT results at $\lambda = 2$, as illustrated in Fig. 5.

D. Polaronic regime, $\lambda \gtrsim 1$

The increase of spectral weight associated to the ordering of polarons is best visualized by analyzing the inte-

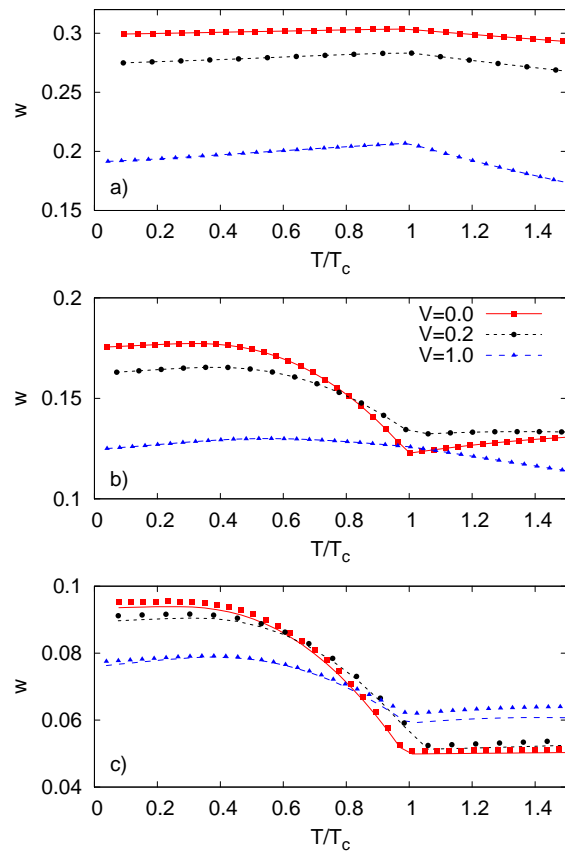


FIG. 6: Total optical weight W as defined in Eq (21), for $\lambda = 0.4$ (a), $\lambda = 1$ (b) and $\lambda = 2$ (c), at different values of V (the legend is indicated in panel b). Lines in panels (a) and (b) are guides to the eye, while in panel (c) they correspond to the analytical strong coupling approximation obtained by integrating Eqs. (B7) and (B8) down to a cutoff frequency equal to T .

grated optical conductivity W defined in Eq. (21), which is proportional to (minus) the total kinetic energy of the interacting system. This is done in Fig. 6. Upon lowering the temperature, the curve corresponding to $\lambda = 2$ and $V = 0$ in Fig. 6.c first decreases (in the normal phase) and then exhibits a sharp increase (in the ordered phase), saturating at $T \ll T_c$ to a value which is about twice the normal phase value. Therefore, at large λ the critical temperature corresponds to a *minimum* of W , which remains true in all the polaronic regime down to the polaron crossover at $\lambda \sim 1$. This is opposite to the usual behavior of charge density waves, where upon lowering the temperature the optical weight first increases and then decreases, reaching a *maximum* at the critical temperature. Such conventional behavior is recovered at small λ , as illustrated in Fig. 6.a for $\lambda = 0.4$.

By following the evolution of the spectral weight from Fig. 6.a to c, it is interesting to see that at intermediate values of the electron-lattice coupling (but still in the polaronic regime), the two competing trends evidenced

above lead to a non-monotonic temperature dependence of the spectral weight even within the CO phase (see in particular the curve labeled $V = 0$ at $\lambda = 1$ in Fig. 6.b). Note that a non-monotonic behavior of the kinetic energy analogous to the one described here was recently observed in the ordered phase of the Falicov-Kimball model at intermediate U .²²

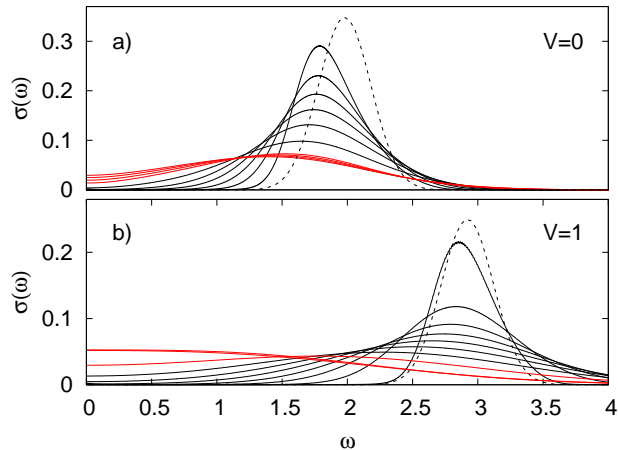


FIG. 7: (color online) Optical conductivity at $\lambda = 1$, $V = 0$ (a) and $V = 1.0$ (b). The curves in panel (a) are at equally spaced temperatures in the range $T/T_c = 0.2 - 1.5$ ($T_c = 0.052D$) and in panel (b) $T/T_c = 0.04 - 1.1$ ($T_c = 0.25D$). Curves corresponding to the disordered phase at $T > T_c$ are in red. The dashed line is the strong coupling result Eq. (B7) at the lowest temperature.

The above spectral weight analysis suggests that both features characteristic of the weak- and strong-coupling limits coexist in the polaronic regime at $\lambda \gtrsim 1$. We can check in Fig. 7.a ($\lambda = 1$, $V = 0$) that such coexistence also naturally manifests in the optical spectra. Here, as in the strong-coupling limit of Fig. 5.a, the polaronic nature of the carriers is testified by the presence of a broad finite-frequency peak already in the normal phase. In this case, however, where the polaron energy E_P is comparable with the free electronic bandwidth D , the peak position lies well below the strong-coupling estimate $2E_P$. Also the shape and width of the peak deviate from the strong-coupling estimate, being both controlled by the ratio s/D (the usual symmetric gaussian shape is recovered as $s \gg D$, see Ref. 36). Most interesting however is the evolution of the optical absorption below T_c , which shares similarities with both behaviors shown in Figs. 4.a and 5.a. Indeed, at intermediate values of the electron-phonon coupling, the optical absorption in the ordered phase exhibits both a marked enhancement and an appreciable transfer of spectral weight to higher frequencies. This composite behavior gives rise to an “isosbestic” region at frequencies below the polaron peak, where the optical absorption is almost independent of temperature.

It was observed by analyzing the phase diagram in Sec.

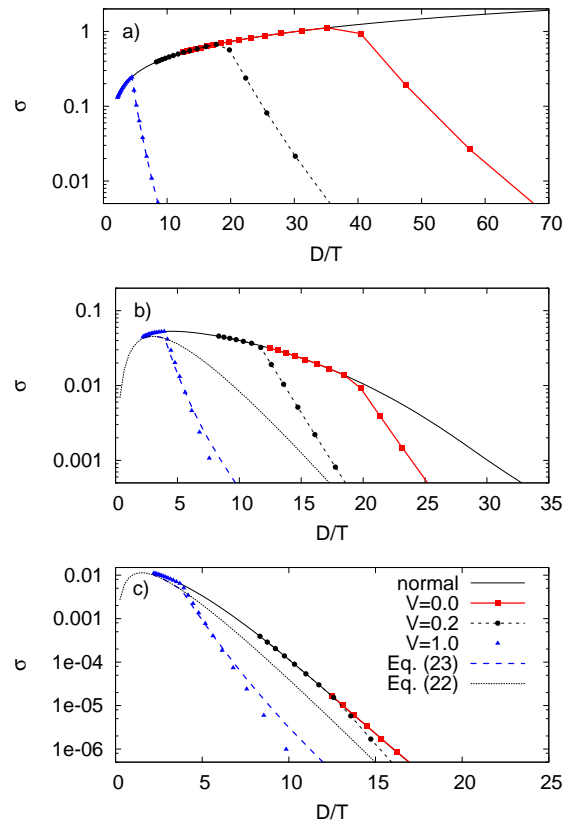


FIG. 8: d.c. conductivity for $\lambda = 0.4$ (a), $\lambda = 1$ (b) and $\lambda = 2$ (c), for different values of V . Lines are guides to the eye, except for $V = 1$ in panels (b) and (c), where the line is the strong coupling formula Eq. (24). The full black line is the DMFT result obtained in the normal phase, and the thin dashed line is the standard polaronic expression Eq. (23).

II that the intersite repulsion V effectively pushes the system towards the weak electron-lattice coupling regime. This conclusion is also supported by the behavior of the optical conductivity spectra. For example, we see from Fig. 1 that at $\lambda = 1$, a repulsion $V = 1$ is sufficient to move the system outside the polaronic phase. Accordingly, the polaron peak that was present at high temperature in Fig. 7.a has disappeared in the $V = 1$ spectrum of Fig. 7.b, and a more conventional gap opening is restored below T_c . If instead one starts from the strong coupling value $\lambda = 2$, an appreciable transfer spectral of spectral weight below the transition is recovered for $V = 1$, as well as a non monotonic behavior of the total spectral weight W (see Fig. 5.b and Fig.6.c).

IV. D.C. CONDUCTIVITY

In this section we briefly describe the d.c. conductivity, which is obtained from the previously derived Kubo formula Eq. (13), by taking the limit $\omega \rightarrow 0$. The numerical results for $\sigma_{d.c.}$ across the CO transition are shown

in Fig. 8 for different values of V , at $\lambda = 0.4$ (a), $\lambda = 1$ (b) and $\lambda = 2$ (c). These values are the same as analyzed in the preceding Section, and correspond respectively to the weak, intermediate and to the strong electron-lattice coupling regime. The CO transition can be clearly identified as a knee in all the conductivity curves, except for $\lambda = 2, V = 0$ (in that case T_c falls outside the range of Fig. 8.c) In the weak coupling regime (Fig. 8.a), the opening of a gap changes the mobility from metallic-like to insulating-like, i.e. the slope of $\sigma_{d.c.}(T)$ changes sign. The changes in the transport properties at the CO transition become less marked in the polaronic regime. In this case the mobility is already thermally activated in the normal phase, and the CO transition only causes an increase of the activation barrier, which is reflected in a change of slope in the Arrhenius plots of Figs. 8.b and Fig. 8.c.

An expression for the d.c. conductivity valid in the strong coupling limit is derived in Appendix B. In the normal phase, one recovers the usual formula for the polaronic activated behavior:

$$\sigma_{d.c.}^{norm}(T) = \frac{\sigma_0}{32\sqrt{2\pi}E_P T^{3/2}} e^{-E_P/2T}. \quad (23)$$

At temperatures below T_c , this generalizes to

$$\sigma_{d.c.}(T) = 4n_d(1 - n_d)\sigma_{d.c.}^{norm}(T). \quad (24)$$

We see that the ordering transition reduces the conductivity in a way that is once again related to the suppression of defects, being proportional to the product of the occupations in the two sublattices, namely $4n_d(1 - n_d) \simeq 1 - \Delta n^2$.

It should be stressed that standard approaches that incorporate Coulomb interactions into the polaronic conductivity would predict an additive contribution $V\Delta n/2$ to the activation barrier at the CO transition,³⁹ which naturally arises from the extra energy cost that a polaron in the majority sublattice has to overcome to hop to a neighboring unoccupied site. While such contribution is indeed recovered in our treatment [see Eq. (B13) in Appendix B], we see here that the dominant conduction mechanism at finite temperatures is related to the presence of charge defects. Being already thermally excited onto the minority sublattice, such defects do not pay an extra cost in Coulomb energy when hopping from site to site, and their motion is therefore more advantageous than ordinary hopping across the gap (remind that at large λ the number of defects n_d does not depend explicitly on V , as was shown in Fig. 3).

Eq. (24) is compared with the full DMFT results for $\lambda = 1, V = 1$ and $\lambda = 2, V = 1$ in Fig. 8.b and Fig. 8.c respectively. It should be stressed that the strong coupling analysis underlying Eqs. (23) and (24) above is strictly valid only at $\lambda \rightarrow \infty$, as it neglects corrections proportional to D in the activation barrier. As a result, the above formulas widely underestimate the electrical conductivity,³⁸ and the agreement with the DMFT data at finite λ and $V = 0$ is not as good as the one obtained

for $\sigma(\omega)$ in the preceding Section. This is particularly evident when comparing Eq. (23) with the $\lambda = 1$ data of Fig. 8.b, where large deviations arise especially at low temperatures $T \ll E_P$. Increasing V shifts the ordering transition to higher temperatures, apparently improving the accuracy of the approximation.

V. DISCUSSION AND CONCLUSIONS

We have calculated the optical and electrical transport properties in a model describing charge ordering in systems with strong electron-lattice interactions. The DMFT treatment used here properly accounts for fluctuations of the lattice polarization. This allows to understand the role played by charge defects in the electrodynamic response of the polaronic ordered phase. The effects of a moderate intersite Coulomb repulsion term, which is often present in interacting narrow-band systems, have also been incorporated.

In the weak electron-phonon coupling regime, we have seen in Sec. II that lattice fluctuations play an important role as soon as $\lambda > 0$, as they strongly reduce the critical temperature compared to the mean-field BCS-like expectation.^{23,26} Our results show that these fluctuations also manifest in the spectral properties, as they provide a disordered effective medium that scatters the electron motion, leading to an appreciable broadening of the sharp spectral features predicted by mean-field theory.

The effects of lattice fluctuations are however much more dramatic in the strong coupling regime, where the charge ordering transition occurs in a polaronic phase with a preexisting local charge segregation. In that case, polaron formation moves most of the spectral weight to a finite frequency absorption peak, whose position hardly changes at the ordering transition. Instead, the distinctive signature of charge ordering in the strong coupling limit is a marked enhancement of the polaronic absorption peak, that is directly related to the suppression of charge defects, i.e. charges promoted to the “wrong” sublattice by the thermal fluctuations. In the polaronic ordered phase, such defects also govern the transport properties, as their motion dominates over the usual hopping mechanism across the dimerization gap. The competing scenarios described above appear to coexist at intermediate electron-lattice interactions ($\lambda \gtrsim 1$), i.e. precisely in the region of the phase diagram where the critical temperature is maximum. In this region, polaronic charge ordering reveals in the optical spectra through both a transfer of spectral weight to high frequencies and a global spectral weight enhancement as the temperature is lowered below T_c .

It should be noted that a model very similar to the one studied here was developed in a series of papers by Ihle and Lorenz,^{39,40,41} and was applied to the long-standing problem of the Verwey transition in Fe_3O_4 — a prototypical example of polaron ordering (see also the review paper Ref. 20). In these works the model Eq. (1) was

solved relying on the anti-adiabatic approximation for the lattice degrees of freedom, where the phonon dynamics is assumed to be faster than the electrons. Our adiabatic treatment can therefore be considered as complementary to the one of Refs. 40,41. While the present approach clearly gives more insight into the physics of charge defects, our classical treatment of phonons has an important limitation that one should keep in mind when attempting a comparison with actual experiments. The results obtained here are expected to apply at temperatures and frequencies larger than the frequency scale of the phonons involved in the CO transition. Properly accounting for the quantum nature of the phonons would restore the possibility of a coherent transport regime at low temperatures,³⁸ and allow for the presence of charge defects even at zero temperature.⁴³

Acknowledgements.

The authors acknowledge useful discussions with L. Benfatto, E. Cappelluti, G. Sangiovanni and A. Toschi.

APPENDIX A: MEAN-FIELD TREATMENT OF THE OPTICAL CONDUCTIVITY.

We evaluate here the optical absorption in the CO state at mean-field level, which applies to the weak electron-lattice coupling limit. This treatment also describes accurately the numerical data at any finite V at nonzero temperature when $\lambda = 0$, due to the intrinsic mean-field treatment of non-local interactions in DMFT. The mean-field solution for the electron propagators is obtained by inverting the matrix

$$\hat{G}_{\mathbf{k}}^{-1} = \begin{pmatrix} \omega + \Delta & -\epsilon_{\mathbf{k}} \\ -\epsilon_{\mathbf{k}} & \omega - \Delta \end{pmatrix} \quad (\text{A1})$$

where Δ is the CO gap, which is determined self-consistently.²³ It is related to the charge dimerization by $\Delta = (\lambda D + V/2)\Delta n$.

The corresponding spectral functions are delta functions, which allow for a direct evaluation of Eq. (13) for a generic DOS. The finite-frequency part, corresponding to interband transitions (across the gap) reads

$$\sigma(\omega) = \frac{\sigma_0 N\phi}{2} \frac{\left(\frac{1}{2}\sqrt{\omega^2 - (2\Delta)^2}\right) (2\Delta)^2}{\sqrt{\omega^2 - (2\Delta)^2} \omega^2} \tanh\left(\frac{\omega}{4T}\right) \quad (\text{A2})$$

which has a square-root singularity at $\omega = 2\Delta$ (the optical gap) followed by a power-law decay at higher frequencies. At finite temperature, states are thermally excited across the gap, which enables the possibility of intraband absorption. In the absence of additional inelastic scatter-

ing mechanisms, this gives rise to a zero-frequency peak:

$$\sigma_D(\omega) = \sigma_0 \delta(\omega) \int_{RBZ} d\epsilon N(\epsilon) \phi(\epsilon) \frac{2\epsilon^2}{\epsilon^2 + \Delta^2} [-f'(\epsilon^2 + \Delta^2)]. \quad (\text{A3})$$

APPENDIX B: STRONG COUPLING APPROXIMATION TO $\sigma(\omega)$

We derive here analytical approximations to Eqs. (5), (14) and (21) that are valid in the strong coupling limit $\lambda \gg 1$.

1. Normal state

Let us first note that the usual strong-coupling formula of Reik³⁷ for the optical conductivity is recovered in the normal phase if we take the atomic limit ($t = 0$) in the propagators appearing in Eq. (13). Indeed, by setting $G_0^{-1} = \omega + i\delta$ it can be shown that the lattice PDF is a sum of two gaussians centered at $\pm g/2k$, each one carrying a weight $n_A = n_B = 1/2^{23}$ (as was mentioned above, the Coulomb interaction term does not affect the properties of the normal phase at mean-field level). This can be cast in the form

$$P_{norm}(X) = g \frac{\cosh(\beta g X/2)}{\sqrt{4\pi E_P T}} e^{-\frac{(gX)^2 + E_P^2}{4E_P T}} \quad (\text{B1})$$

with the polaron energy defined as $E_P = g^2/2k = \lambda D$. The spectral function is obtained straightforwardly from Eq. (B1) through the relation $\rho_{norm}(\omega) = P_{norm}(\omega/g)/g$ [cf. Eq. (5)].

Since in this limit the electron Green's function is site diagonal and momentum-independent, the ϵ -integration can be factored out from Eq. (13), yielding a prefactor $\int d\epsilon N(\epsilon)\phi(\epsilon) = 1/4$ on the Bethe lattice. The remaining frequency integral can be performed using the relation

$$[f(\omega + \nu) - f(\nu)] = \frac{\sinh[\frac{\beta\omega}{2}]}{2 \cosh[\frac{\beta(\omega+\nu)}{2}] \cosh[\frac{\beta\nu}{2}]} \quad (\text{B2})$$

which leads to the desired result

$$\sigma(\omega) = \frac{\sigma_0}{\sqrt{2\pi E_P T}} \frac{\sinh(\beta\omega/2)}{16\omega} e^{-\frac{\omega^2 + 4E_P^2}{8E_P T}}. \quad (\text{B3})$$

Focusing on the finite frequency part $\omega \gg T$, this can be further simplified to

$$\sigma_{norm}(\omega) = \frac{\sigma_0}{32\omega\sqrt{2\pi E_P T}} e^{-\frac{(\omega - 2E_P)^2}{8E_P T}}. \quad (\text{B4})$$

This formula represents a modified gaussian absorption band having its maximum at $\omega = 2E_P$ and a width

$\sqrt{2}s = 2\sqrt{E_P T}$, which reflects the thermal fluctuations of the phonon field that couples to the electron motion. Note that if the phonon quantum fluctuations are correctly taken into account, the width of the absorption band does not shrink indefinitely at low temperatures, but rather saturates to a finite value $s^2 = 2E_P\omega_0$.³⁶ One can observe that the numerical factor $1/32$ in Eq. (B4) implicitly includes the density dependent factor $n(1-n)$ expected from theories of independent polarons.

2. Charge ordered state

In the charge ordered state ($\Delta n \neq 0$), the two contributions to the lattice PDF are unbalanced by a factor which takes into account the different fillings $n_A \neq n_B$ on nonequivalent sublattices. As a result, Eq. (B1) becomes

$$P_{A,B}(X) = P_{norm}(X)[1 \pm (1 - 2n_d) \tanh(\beta g X/2)] \quad (\text{B5})$$

where the $+$ and $-$ signs correspond to the A and B sublattices respectively. The lattice PDF is again the sum of two gaussian peaks, centered at the minima $\pm X_0$ of the adiabatic potentials $V_{A,B}$, whose weights are now respectively n_d and $1 - n_d$. At $\lambda = 2$, this approximation compares very well with the full DMFT result illustrated in Fig. 2. That figure also shows that for moderate $V \lesssim 1$ the shape of the gaussian peaks in the PDF is unaffected by the electrostatic repulsion, which only enters implicitly through the self-consistent determination of n_d .

From Eq. (B5) we obtain the spectral function for the two sublattices:

$$\begin{aligned} \rho_A(\omega) &= (1 - n_d) g_+ \left(\omega + \frac{V\Delta n}{2} \right) + n_d g_- \left(\omega + \frac{V\Delta n}{2} \right) \\ \rho_B(\omega) &= n_d g_+ \left(\omega - \frac{V\Delta n}{2} \right) + (1 - n_d) g_- \left(\omega - \frac{V\Delta n}{2} \right) \end{aligned}$$

where

$$g_\alpha(\omega) = \frac{1}{\sqrt{2\pi s^2}} \exp\left(-\frac{\omega - \alpha E_P}{2s^2}\right) \quad (\text{B6})$$

and $\alpha = \pm 1$.

Taking the low temperature limit ($T \ll \sqrt{E_P T}, D$) in Eq. (13) and using the spectral functions above, it is possible to obtain an expression for the finite frequency conductivity ($\omega \gg T$). At $V = 0$ it takes the simple form:

$$\sigma(\omega) = 2[1 - 2n_d(1 - n_d)]\sigma_{norm}(\omega) \quad (\text{B7})$$

which directly relates the observed enhancement of the optical absorption in the CO phase, in agreement with the general arguments presented in Sec. III C. In the presence of intersite repulsion, the above formula gener-

alizes to

$$\sigma(\omega) = \frac{\sigma_0}{16\omega\sqrt{2\pi E_P T}} \left[e^{-\frac{(\omega - 2E_P - V\Delta n)^2}{8E_P T}} (1 - n_d)^2 + e^{-\frac{(\omega - 2E_P + V\Delta n)^2}{8E_P T}} (n_d)^2 \right], \quad (\text{B8})$$

which clearly reduces to Eq. (B7) when $V = 0$. Both expressions compare well with the numerical data of Fig. 5 at $\lambda = 2$. Moreover, the total optical spectral weight obtained by integrating Eq. (B8) down to a cutoff frequency $\omega = T$ correctly reproduces the non-monotonic temperature dependence of the DMFT results shown in Fig. 6.c. Note that at extremely large V , this expression predicts a double-peak structure, which is not observed in the numerical data at moderate V .

The results presented in this Appendix, derived under the assumption of a vanishing bandwidth, are strictly valid as long as $s \gg D$.³⁶ From the asymptotic strong coupling expression $T_c = D/(16\lambda) + V/4$ we can estimate

$$\frac{s}{D} \Big|_{T_c} \simeq \frac{1}{2^{3/2}} \sqrt{1 + 4\lambda \frac{V}{D}}. \quad (\text{B9})$$

We see that at $V = 0$ the condition $s \gg D$ is never realized in the relevant region around T_c , and some finite bandwidth corrections to the polaronic lineshapes can be expected.³⁶ Examination of Figs. 5 and 7 shows that the accuracy of the strong coupling formula Eq. (B7) improves when an explicit Coulomb term V is included.

3. d.c. conductivity

The d.c. conductivity is obtained by taking the limit $\omega \rightarrow 0$ in Eq. (13). Some care must be taken in integrating the gaussian spectral functions in the presence of the factor $1/[4T \cosh(\nu/2T)]$ originating from the Fermi functions. For $T \ll E_P$ one obtains

$$\begin{aligned} \sigma_{d.c.}(T) &= \frac{\sigma_0}{16\pi E_P T} e^{-\frac{E_P}{2T} - \frac{(V\Delta n)^2}{8E_P T}} \times \\ &\times \left[2n_d(1 - n_d) \sqrt{\frac{\pi E_P}{2T}} + (1 - n_d)^2 e^{-\frac{V\Delta n}{2T}} + n_d^2 e^{\frac{V\Delta n}{2T}} \right]. \end{aligned} \quad (\text{B10})$$

which reduces in the normal phase to the usual formula for the polaronic conductivity:

$$\sigma_{d.c.}^{norm}(T) = \frac{\sigma_0}{32\sqrt{2\pi E_P T^{3/2}}} e^{-E_P/2T}. \quad (\text{B11})$$

In the CO state at temperatures $T \lesssim T_c$, the leading contribution to Eq. (B10) is

$$\sigma_{d.c.}(T) = 4n_d(1 - n_d) e^{-\frac{(V\Delta n)^2}{8E_P T}} \sigma_{d.c.}^{norm}(T). \quad (\text{B12})$$

which shows that the dominant conduction mechanism in the polaronic ordered phase involves thermally activated defects. The exponential term is close to 1 at moderate values of V such as the ones studied here, and can be dropped. This expression breaks down as $T \ll T_c$, when the number of defects n_d vanishes. In this case a more conventional result is recovered

$$\sigma_{d.c.}(T) = \frac{\sigma_0}{16\pi E_P T} e^{-\frac{(E_P + V\Delta n/2)^2}{2E_P T}}. \quad (\text{B13})$$

This formula predicts an additive contribution $V\Delta n/2$ to the activation barrier, corresponding to the extra energy cost that a polaron has to overcome when hopping to its neighboring sites.³⁹

APPENDIX C: F-SUM RULE IN THE BROKEN-SYMMETRY PHASE

In this section we demonstrate the f-sum rule for the optical conductivity evaluated through the DMFT formula Eq. (13), generalizing the demonstration of Ref. 42 to the broken-symmetry phase. We first rewrite the integral of the optical conductivity in the form

$$\int_0^\infty \sigma(\omega) = \frac{\sigma_0}{2} \int_{RBZ} d\epsilon N(\epsilon) \phi(\epsilon) I(\epsilon), \quad (\text{C1})$$

with

$$I(\epsilon) = \frac{1}{\pi^2} \int_{-\infty}^\infty d\nu \int_{-\infty}^\infty d\nu' \frac{f(\nu) - f(\nu')}{\nu' - \nu} \text{Tr} \left[\sigma_x \text{Im} \hat{G}_\epsilon(\nu') \sigma_x \text{Im} \hat{G}_\epsilon(\nu) \right]. \quad (\text{C2})$$

This expression can be transformed to

$$\begin{aligned} I(\epsilon) &= \frac{1}{\pi} \int_{-\infty}^\infty d\nu f(\nu) \text{Tr} \left[2\sigma_x \text{Im} \hat{G}_\epsilon(\nu) \sigma_x \text{Re} \hat{G}_\epsilon(\nu) \right] \\ &= \frac{\text{Tr}}{\pi} \int_{-\infty}^\infty d\nu f(\nu) \text{Im} \left[\sigma_x \hat{G}_\epsilon(\nu) \sigma_x \hat{G}_\epsilon(\nu) \right] \\ &= \frac{\text{Tr}}{\pi} \int_{-\infty}^\infty d\nu f(\nu) \text{Im} \left[\sigma_x \frac{d\hat{G}_\epsilon(\nu)}{d\epsilon} \right]. \end{aligned}$$

The latter equality is obtained using the fact that $d(\hat{G}_\epsilon^{-1} \hat{G}_\epsilon)/d\epsilon = d(1)/d\epsilon = 0$ and observing that from Eq. (9) one has $d\hat{G}_\epsilon^{-1}/d\epsilon = -\sigma_x$. Going back to Eq. (C1) and integrating by parts yields

$$\int_0^\infty \sigma(\omega) = \sigma_0 \int_{RBZ} d\epsilon \frac{d(N\phi)}{d\epsilon} \int d\nu f(\nu) 2\rho_\epsilon^{AB}(\nu). \quad (\text{C3})$$

With the present choice of the current vertex $\phi(\epsilon)$ for the Bethe lattice one has $\frac{dN\phi}{d\epsilon} = -\epsilon N(\epsilon)$ so that the above expression reduces to

$$\int_0^\infty \sigma(\omega) = -\frac{\sigma_0}{2} K \quad (\text{C4})$$

where K is the total kinetic energy defined as

$$K = \int_{RBZ} d\epsilon N(\epsilon) \epsilon \int d\nu f(\nu) 2\rho_\epsilon^{AB}(\nu). \quad (\text{C5})$$

¹ G. Grüner, *Density Waves in Solids*, Addison-Wesley Publishing Company, 1994.

² D. S. Dessau et al., *Phys. Rev. Lett.* 81, 192 (1998)

³ C. P. Adams et al., *Phys. Rev. Lett.* 85, 3954 (2000)

⁴ L. Vasiliu-Doloc, S. Rosenkranz, R. Osborn, S.K. Sinha, J.W. Lynn, J. Mesot, O.H. Seeck, G. Preosti, A.J. Fedro, and J.F. Mitchell, *Phys. Rev. Lett.* 83, 4393 (1999)

⁵ T. Katsufuji et al., *Phys. Rev. B* 54, R14230 (1996).

⁶ P. Calvani, A. Paolone, P. Dore, S. Lupi, P. Maselli, P. G. Medaglia, S-W. Cheong, *Phys. Rev. B* 54, R9592 (1996)

⁷ C. Bernhard, A.V. Boris, N. N. Kovaleva, G. Khaliullin, A.V. Pimenov, Li Yu, D. P. Chen, C.T. Lin, and B. Keimer. *Phys. Rev. Lett* 93, 167003 (2004)

⁸ N. L.Wang, Dong Wu, G. Li, X. H. Chen, C. H. Wang, and X.G. Luo, *Phys. Rev. Lett.* 93, 147403 (2005)

⁹ L. Degiorgi, P. Wachter and D. Ihle, *Phys. Rev. B* 35, 9259

(1987)

¹⁰ S. K. Park, T. Ishikawa, and Y. Tokura, *Phys. Rev. B* 58, 3717 (1998)

¹¹ D. Schrupp et al., *Europhys. Lett.* 70, 789 (2005)

¹² C. Presura, M. Popinciuc, P. H. van Loosdrecht, D. van der Marel, M. Mostovoy, T. Yamauchi, and Y. Ueda, *Phys. Rev. Lett.* 90, 026402 (2003)

¹³ L. Baldassarre, A. Perucchi, E. Arcangeletti, D. Nicoletti, D. Di Castro, P. Postorino, V. A. Sidorov, and S. Lupi *Phys. Rev. B* 75, 245108 (2007)

¹⁴ J. P. Attfield, A. M. T. Bell, L. M. Rodriguez-Martinez, J. M. Greneche, R. J. Cernik, J. F. Clarke & D. A. Perkins, *Nature* 396, 655 (1998)

¹⁵ L. Perfetti, H. Berger, A. Reglinelli, L. Degiorgi, H. Hochst, J. Voit, G. Margaritondo, and M. Grioni, *Phys. Rev. Lett.* 87, 216404 (2001)

- ¹⁶ L. Perfetti, S. Mitrovic, G. Margaritondo, M. Grioni, L. Forro, L. Degiorgi, and H. Hochst, Phys. Rev. B 66, 075107 (2002).
- ¹⁷ R. Pietig, R. Bulla, S. Blawid, Phys. Rev. Lett. 82, 4046 (1999)
- ¹⁸ N.-H. Tong, S.-Q. Shen, R. Bulla, Phys. Rev. B 70, 085118 (2004)
- ¹⁹ M. Daghofer, R. M. Noack, P. Horsch, preprint arXiv:0711.1990
- ²⁰ F. Walz, J. Phys. Cond. Matter 14, R285 (2002)
- ²¹ S. R. Hassan and H. R. Krishnamurthy, Phys. Rev. B 76, 205109 (2007)
- ²² O. P. Matveev, A. M. Shvaika, J. K. Freericks, Phys. Rev. B 77, 035102 (2008)
- ²³ S. Ciuchi and F. de Pasquale, Phys. Rev. B 59, 5431 (1999)
- ²⁴ C. A. Perroni, V. Cataudella, G. De Filippis, G. Iadonisi, V. Marigliano Ramaglia, and F. Ventriglia, Phys. Rev. B 67, 094302 (2003)
- ²⁵ S. Fratini and G. Rastelli, Phys. Rev. B 75, 195103 (2007)
- ²⁶ S. Blawid and A. Millis, Phys. Rev. B 62, 2424 (2000)
- ²⁷ A. Georges et al., Rev. Mod. Phys. 68, 13 (1996).
- ²⁸ A. Khurana, Phys. Rev. Lett. 64, 1990 (1990).
- ²⁹ H. Schweitzer and G. Czycholl, Phys. Rev. Lett. 67, 3724 (1991)
- ³⁰ Th. Pruschke, D. L. Cox, and M. Jarrell, Phys. Rev. B 47, 3553 (1993)
- ³¹ W. Chung and J. K. Freericks, Phys. Rev. B 57, 11955 (1998).
- ³² A. Chattopadhyay, A. J. Millis, and S. Das Sarma, Phys. Rev. B 61, 10738 (2000).
- ³³ S. Fratini and S. Ciuchi, Phys. Rev. 72, 235107 (2005)
- ³⁴ This estimate is valid outside the polaronic crossover region. Approaching the polaron crossover coupling both from above and below the CO temperature, the local displacements strongly deviate from the gaussian behaviour.
- ³⁵ A. J. Millis, R. Mueller and B. I. Shraiman, Phys. Rev. B 54, 5389 (1996)
- ³⁶ S. Fratini and S. Ciuchi, Phys. Rev. B 74, 075101 (2006)
- ³⁷ H. G. Reik, Solid State Commun. 1, 102 (1963)
- ³⁸ S. Fratini and S. Ciuchi Phys. Rev. Lett. 91, 256403 (2003)
- ³⁹ D. Ihle, Z. Phys. B 58, 91 (1985)
- ⁴⁰ D. Ihle and B. Lorentz, J. Phys. C: Solid State Phys. 18, L647 (1985)
- ⁴¹ D. Ihle and B. Lorentz, J. Phys. C: Solid State Phys. 19, 5239 (1986)
- ⁴² N. Blümer, Ph.D Thesis, Univ. Augsburg (2003)
- ⁴³ S. Blawid and A. J. Millis, Phys. Rev. B 63, 115114 (2001)
- ⁴⁴ A BCS-like prediction $T_c \propto \exp(-const/\lambda)$, valid in the limit $\lambda \rightarrow 0$, actually overestimates the critical temperature at any finite λ since it neglects the possible fluctuations of the order parameter, see Refs. 23,26